

# A revised $B(E2; 2_1^+ \rightarrow 0_1^+)$ value in the semi-magic nucleus $^{210}\text{Po}$

D. Kocheva<sup>1,a</sup>, G. Rainovski<sup>1</sup>, J. Jolie<sup>2</sup>, N. Pietralla<sup>3</sup>, A. Blazhev<sup>2</sup>, A. Astier<sup>4</sup>, R. Altenkirch<sup>2</sup>, S. Ansari<sup>2</sup>, Th. Braunroth<sup>2</sup>, M.L. Cortés<sup>3</sup>, A. Dewald<sup>2</sup>, F. Diel<sup>2</sup>, M. Djongolov<sup>1</sup>, C. Fransen<sup>2</sup>, K. Gladnishki<sup>1</sup>, A. Hennig<sup>2</sup>, V. Karayonchev<sup>2</sup>, J.M. Keatings<sup>5</sup>, E. Kluge<sup>2</sup>, J. Litzinger<sup>2</sup>, C. Müller-Gatermann<sup>2</sup>, P. Petkov<sup>6</sup>, M. Rudigier<sup>2</sup>, M. Scheck<sup>5</sup>, Ph. Scholz<sup>2</sup>, P. Spagnoletti<sup>5</sup>, M. Spieker<sup>2</sup>, C. Stahl<sup>3</sup>, R. Stegmann<sup>3</sup>, M. Stoyanova<sup>1</sup>, P. Thöle<sup>2</sup>, N. Warr<sup>2</sup>, V. Werner<sup>3</sup>, W. Witt<sup>3</sup>, D. Wölk<sup>2</sup>, K.O. Zell<sup>2</sup>, P. Van Isacker<sup>7</sup>, and V.Yu. Ponomarev<sup>3</sup>

<sup>1</sup> Faculty of Physics, St. Kliment Ohridski University of Sofia, 1164 Sofia, Bulgaria

<sup>2</sup> Institut für Kernphysik, Universität zu Köln, 50937 Cologne, Germany

<sup>3</sup> Institut für Kernphysik, Technische Universität Darmstadt, 64289 Darmstadt, Germany

<sup>4</sup> CSNSM, IN2P3/CNRS and Université Paris-Sud, F-91405 Orsay Campus, France

<sup>5</sup> School of Engineering & Computing, University of the West of Scotland, PA1 2BE Paisley, UK

<sup>6</sup> National Institute for Physics and Nuclear Engineering, 77125 Bucharest-Magurele, Romania

<sup>7</sup> Grand Accélérateur National d'Ions Lourds, CEA/DRF-CNRS/IN2P3, Bd. Henri Becquerel BP 55027, F-14076 Caen, France

Received: 23 June 2017 / Revised: 25 July 2017

Published online: 7 September 2017 – © Società Italiana di Fisica / Springer-Verlag 2017

Communicated by N. Kalantar-Nayestanaki

**Abstract.** The lifetimes of the  $2_1^+$ , the  $2_2^+$  and the  $3_1^-$  states of  $^{210}\text{Po}$  have been measured in the  $^{208}\text{Pb}(^{12}\text{C}, ^{10}\text{Be})^{210}\text{Po}$  transfer reaction by the Doppler-shift attenuation method. The result for the lifetime of the  $2_1^+$  state is about three times shorter than the adopted value. However, the new value still does not allow for a consistent description of the properties of the yrast  $2_1^+$ ,  $4_1^+$ ,  $6_1^+$ , and  $8_1^+$  states of  $^{210}\text{Po}$  in the framework of nuclear shell models. Quasi-particle Phonon Model (QPM) calculations also cannot overcome this problem thus indicating the existence of a peculiarity which is neglected in both theoretical approaches.

## 1 Introduction

The low-energy spectra of semi-magic nuclei, especially those with two additional nucleons with respect to a doubly magic core, are of importance because they reveal the basic interactions that play a role in the formation of more complex collective excitations in open-shell nuclei. The properties of semi-magic nuclei are dominated by their single-particle structure and can be well understood in the framework of the nuclear shell model [1,2], which constitutes the standard approach to understand their low-energy spectra. Besides single-particle structure, pairing correlations are crucial in these nuclei because they favour the formation of configurations with nucleons in pairs coupled to angular momentum  $J = 0$ . As a result semi-magic nuclei have low-energy excitations of low “seniority”  $v$ , the quantum number that counts the number of unpaired nucleons [3]. These nuclei display multiplets of states that have the same seniority  $v$ . If the valence nucleons are confined to a single- $j$  orbital, it is known that, to a good approximation, the interaction between identical nucleons conserves seniority [4,5]. If the valence shell con-

sists of several orbitals, a generalized-seniority scheme can be formulated [6], which can be considered as a truncation of the nuclear shell model.

The conservation of seniority imposes a number of simple rules [4,5,7,8] that can be exploited for tracing the evolution from seniority-like behaviour to collectivity with an increasing number of valence nucleons [9,10]. Nuclei with two valence nucleons serve as reference points, providing the properties of the basic  $j^2$  configurations such as the energies of states with  $v = 2$  and the absolute  $E2$  transition strengths for the seniority-changing transition ( $\Delta v = 2$ )  $2_1^+ \rightarrow 0_1^+$  and the seniority-preserving transitions ( $\Delta v = 0$ ) within the  $v = 2$  multiplet. Moreover, these observables can be used for basic tests of complete shell-model calculations.

The semi-magic nucleus  $^{210}\text{Po}$  has two additional protons with respect to the doubly-magic nucleus  $^{208}\text{Pb}$ . The energies of its yrast  $2^+$ ,  $4^+$ ,  $6^+$ , and  $8^+$  states follow a seniority-like pattern of decreasing energy splitting between adjacent states with increasing spin (cf. fig. 1), suggesting that the states belong to the  $(\pi h_{9/2})^2$  multiplet. Data on absolute strengths for  $E2$  transitions between these states are also available. The data are extracted from the lifetimes of the  $4^+$ ,  $6^+$  and  $8^+$  levels, which

<sup>a</sup> e-mail: dkocheva@phys.uni-sofia.bg

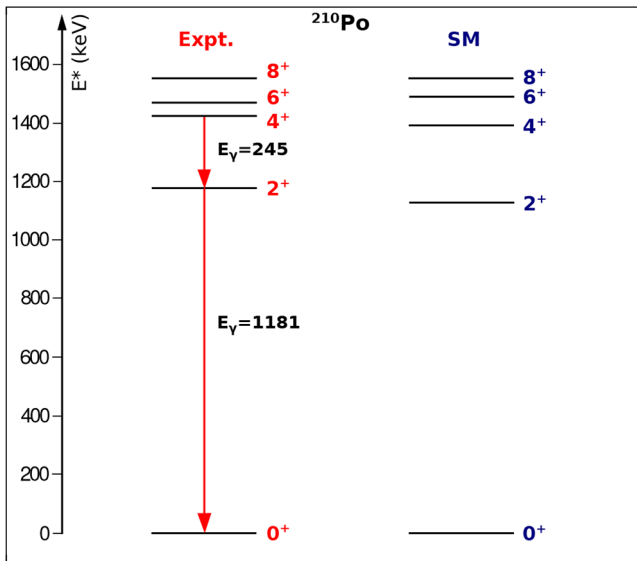


**Fig. 1.** (Color online) Experimental and calculated yrast states of  $^{210}\text{Po}$ . The calculated shell-model levels are taken from ref. [13].

are measured by the electronic timing technique [11]. The  $B(E2; 2_1^+ \rightarrow 0_1^+)$  value is determined from the cross-sections for populating the  $2_1^+$  state in  $^{210}\text{Po}$  in inelastic scattering of deuterons and protons [12]. Large-scale shell-model studies of  $^{210}\text{Po}$  using realistic interactions [13,14] well reproduce the energies of the yrast  $2^+$ ,  $4^+$ ,  $6^+$ , and  $8^+$  levels as can be seen in fig. 1. The calculated wave functions show that the dominant component of the yrast states is the  $(\pi h_{9/2})^2$  configuration, corroborating the expectation that they belong to the seniority  $v = 2$  multiplet. The  $E2$  strengths for the transitions between the  $4^+$ ,  $6^+$  and  $8^+$  states are also almost perfectly reproduced (cf. table VII in ref. [13] and table III in ref. [14]). However, in both studies [13,14] the  $B(E2; 2_1^+ \rightarrow 0_1^+)$  value is overestimated by a factor of six. Such a significant discrepancy between the shell-model calculations and the data is an indication either for an inaccurate experimental value [13,14] or for deficiencies in the model, as suggested in ref. [14]. This has motivated us to perform a model-independent measurement of the lifetime of the  $2_1^+$  level in  $^{210}\text{Po}$  based on the Doppler-shift attenuation method (DSAM) (cf. ref. [15] and references therein) and to seek an alternative theoretical description of the properties of the yrast states of  $^{210}\text{Po}$  in the framework of the Quasi-particle Phonon Model (QPM) [16].

## 2 Experimental set-up

The experiment was performed at the FN Tandem facility of the University of Cologne. Excited states of  $^{210}\text{Po}$  were populated using the  $^{208}\text{Pb}(^{12}\text{C}, ^{10}\text{Be})^{210}\text{Po}$  transfer reaction at a beam energy of 62 MeV. The beam energy

was chosen to be about 2 MeV below the Coulomb barrier. The target was a self-supporting  $10 \text{ mg/cm}^2$  thick Pb foil enriched to 99.14% with the isotope  $^{208}\text{Pb}$ . The reaction took place in the reaction chamber of the Cologne plunger device [17]. In order to detect the recoiling light reaction fragments an array of solar cells was used. The array consisted of six  $10 \text{ mm} \times 10 \text{ mm}$  cells and was placed at a distance of about 15 mm between their centers and the target covering an angular range between  $116.8^\circ$  and  $167.2^\circ$ . The emitted  $\gamma$ -rays were registered by 11 HPGe detectors mounted outside the plunger chamber in two rings at an average distance of 12 cm from the target. Five detectors were positioned at  $142.3^\circ$  with respect to the beam direction and the other six formed a ring at  $35^\circ$ . Data were taken in coincidence mode of at least one solar cell and one HPGe detector (particle- $\gamma$ ) or when at least two HPGe detectors ( $\gamma$ - $\gamma$ ) have fired in coincidence.

## 3 Data analysis and results

The particle- $\gamma$  coincidence data were sorted in two matrices depending on the position of the HPGe detectors. A projection of the particle- $\gamma$  matrix obtained with  $\gamma$ -ray detection at  $142.3^\circ$  is shown in fig. 2(a). The  $\gamma$ -rays in coincidence with the group of particles indicated as “ $^{210}\text{Po}$ ” in fig. 2(a) are shown in fig. 2(b). This spectrum is dominated by the 1181 keV and the 245 keV lines which are the  $\gamma$ -ray transitions depopulating the first two yrast states of  $^{210}\text{Po}$  [18] (cf. fig. 1). Besides some contaminants from  $^{211}\text{Po}$  (which are shown in purple), all other  $\gamma$ -rays in the spectrum in fig. 2(b) originate from the decay of excited states of  $^{210}\text{Po}$ . The 1181, 2290, and 1205 keV  $\gamma$ -ray lines show well-pronounced Doppler shapes which allow us to extract the lifetimes of the  $2_1^+$ , the  $2_2^+$  and the  $3_1^-$  states of  $^{210}\text{Po}$ , respectively.

The line-shape analysis was performed with the integrated software package APCAD (Analysis Program for Continuous Angle DSAM) [19]. In APCAD, the slowing down process is simulated by GEANT4 [20]. The electronic stopping powers were taken from the Northcliffe and Schilling tables [21] with corrections for the atomic structure of the medium, as discussed in ref. [22]. The angular straggling due to nuclear collisions is modelled discretely by means of Monte Carlo simulation while the corresponding energy loss is considered to emerge as a result from a continuous process for which the nuclear stopping powers were taken from SRIM2013 [23] and reduced by 30% [24]. The analysis accounts for the response of the HPGe detectors, for the experimental geometry, and for the restrictions on the reaction kinematics imposed by the solar-cell array. The uncertainties of the results for the lifetimes include statistical uncertainties from the line-shape fits and 10% uncertainty in the nuclear and electronic stopping powers. The software and the approach described above were verified in a previous study [25].

A partial level scheme representing the known transitions directly populating the  $2_1^+$  state of  $^{210}\text{Po}$  [18] is shown in fig. 3. The lifetimes of the  $2_2^+$  state at 2290 keV

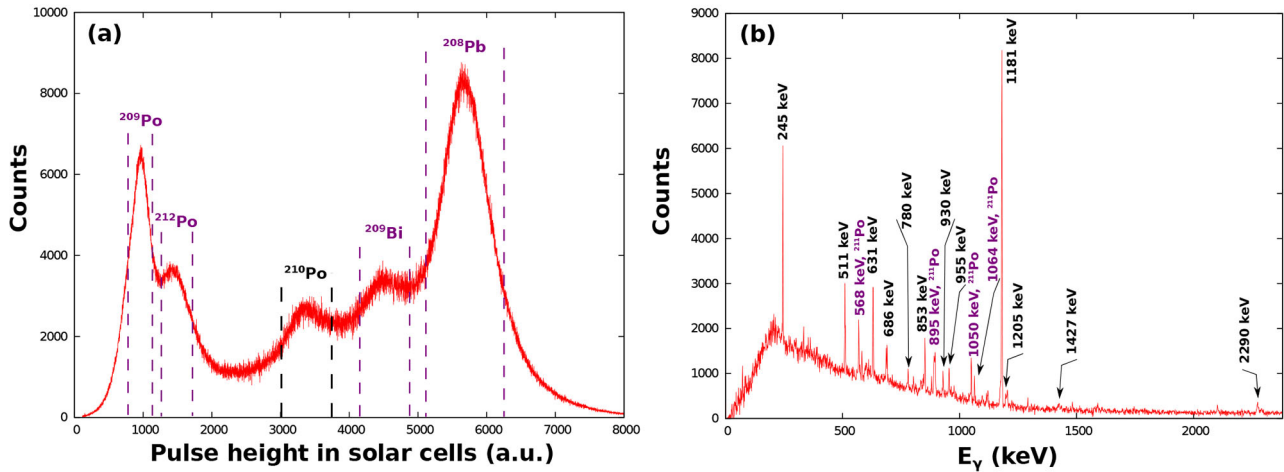


**Fig. 2.** (Color online) (a) The projection of the particle- $\gamma$  matrix obtained by coincidence detection of charged particles in the solar-cell array and a  $\gamma$ -ray at a  $\Theta_\gamma = 142^\circ$  polar angle. The vertical dashed lines represent parts of the particle spectrum found to be in coincidence with  $\gamma$ -rays from the indicated nuclei. (b) The  $\gamma$ -ray spectrum in coincidence with the group of particles indicated as “ $^{210}\text{Po}$ ” in panel (a).

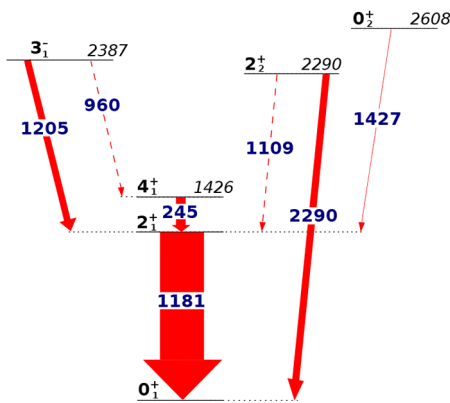


**Fig. 3.** (Color online) Partial level scheme of  $^{210}\text{Po}$  showing the excited states which feed the first  $2^+$  state directly. The thicknesses of the arrows are proportional to the observed  $\gamma$ -ray intensities. The transitions not observed in our data are presented with dashed arrows.

and  $3_1^-$  state at 2387 keV were extracted from the line shapes of the 2290 keV ( $2_2^+ \rightarrow 0_1^+$ ) and the 1205 keV ( $3_1^- \rightarrow 2_1^+$ ) transitions in particle-gated spectra, respectively. These spectra are, in fact,  $\gamma$ -ray singles spectra which, in principle, only contain information for the effective lifetimes. However, due to the reaction mechanism it is justified to consider that slow feeding contributions to the effective lifetimes of excited states of  $^{210}\text{Po}$  can originate only from discrete decays of higher-lying states, as suggested in refs. [26, 27]. The  $\gamma$ - $\gamma$  coincidence data show that the 1205 keV transition is in coincidence with the 1181 keV ( $2_1^+ \rightarrow 0_1^+$ ) transition only, while the 2290 keV ( $2_2^+ \rightarrow 0_1^+$ ) transition is not present in the coincidence data. This observation indicates that the  $2_2^+$  and the  $3_1^-$  states are di-

rectly populated in the transfer reaction. Therefore only fast feeding ( $\tau_{\text{feeding}} \leq 10$  fs) was introduced in the fits of their line shapes. The fits are presented in fig. 4 and the extracted lifetimes are summarized in table 1.

The lifetime of the first excited  $2^+$  state of  $^{210}\text{Po}$  was obtained from the line shape of the 1181 keV ( $2_1^+ \rightarrow 0_1^+$ ) transition. Using the  $\gamma$ - $\gamma$  and the  $\gamma$ -particle coincidence data from our experiment, and the known branching ratios [18] we have estimated that 38% of the feeding of the  $2_1^+$  state originates from the states depicted in fig. 3. The  $\gamma$ - $\gamma$  and the  $\gamma$ -particle coincidence data were used to estimate that the contributions of the 245 keV and the 1205 keV transitions account for 20% and 16%, respectively (cf. fig. 3). We have not observed the 1109 keV ( $2_2^+ \rightarrow 2_1^+$ ) transition in our data. However, the 2290 keV ( $2_2^+ \rightarrow 0_1^+$ ) transition is clearly visible in the  $\gamma$ -particle data (cf. fig. 2(b)) which in combination with the known branching ratio for the decay of the  $2_2^+$  state [18] allowed us to estimate that the feeding to the  $2_1^+$  state via the 1109 keV transition is 2%.

The lifetimes of the  $2_2^+$  and the  $3_1^-$  state (cf. table 1) and their influence of the line shape of the 1181 keV transition were taken into account by the fitting procedure for the lifetime of the  $2_1^+$  state. A special care was taken to account for the impact of the 245 keV ( $4_1^+ \rightarrow 2_1^+$ ) transition. The  $4_1^+$  state of  $^{210}\text{Po}$  is a long-lived state with lifetime  $\tau = 2.21(10)$  ns [11]. Consequently, it always decays at rest in the present experiment. The same is valid for the decays of the  $6_1^+$  and the  $8_1^+$  states (cf. fig. 1). Their lifetimes are even longer than the one for the  $4_1^+$  state [11]. It has to be noted that although we have not observed  $\gamma$ -ray transitions from the decays of the  $6_1^+$  and the  $8_1^+$  states, the population of these states in the present experiment cannot be excluded and their decay could potentially contribute to the yield of the 245 keV transition in the cascade  $8_1^+ \rightarrow 6_1^+ \rightarrow 4_1^+ \rightarrow 2_1^+$  (cf. fig. 1).

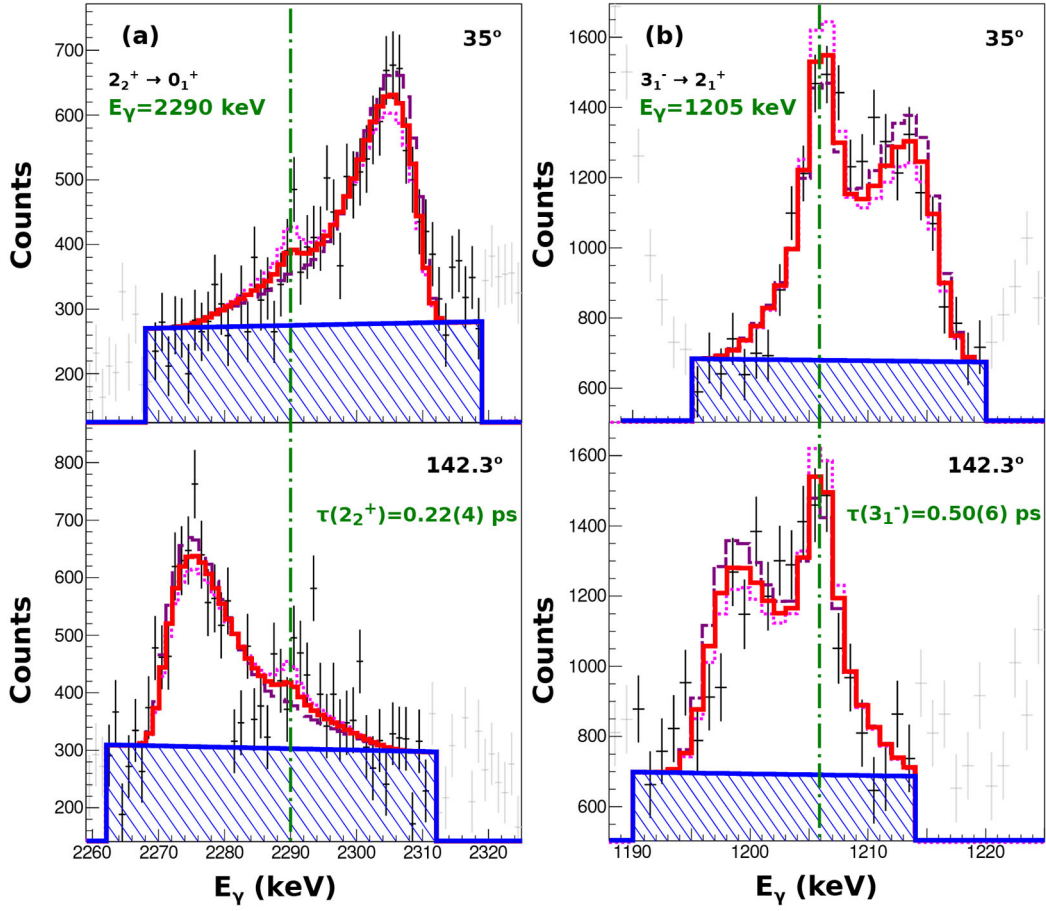


**Fig. 4.** (Color online) An example of line-shape fits of the 2290.1 keV ( $2_2^+ \rightarrow 0_1^+$ ) (a) and the 1205.4 keV ( $3_1^- \rightarrow 2_1^+$ ) (b) transitions. The crossed (blue) areas show the background regions. The solid (red) lines represent the fits corresponding to the adopted lifetimes. The vertical dash-dotted (green) lines show the position of the unshifted peaks. The dashed (violet) and the dotted (pink) lines represent the fits with  $\tau - \sigma$  and  $\tau + \sigma$ , respectively.

**Table 1.** Properties of the three investigated low-lying states of  $^{210}\text{Po}$  and  $\gamma$ -ray transitions originating from their decays. Denoted are: the excitation energies ( $E_{level}$ ); the spin and parity of the initial levels ( $J^\pi$ ) and of the final levels ( $J_{final}^\pi$ ); the  $\gamma$ -ray energies ( $E_\gamma$ ); the relative intensities ( $I_\gamma$ ); the total electron conversion coefficients ( $\alpha$ ); the multipole mixing ratios ( $\delta$ ) of the  $\gamma$ -ray transitions; the lifetimes of the states; the absolute transition strengths.

$E_{level}$ (keV)	$J^\pi$	$J_{final}^\pi$	$E_\gamma$ (keV)	$I_\gamma$ <sup>a</sup> %	$\alpha$ <sup>b</sup>	$\delta$ <sup>c</sup>	$\tau$ (ps)	Transition strength <sup>d</sup> $J^\pi \rightarrow J_{final}^\pi$
1181	$2_1^+$	$0_1^+$	1181	100	0.00535		2.6(4)	$B(E2) = 136(21)$
2290	$2_2^+$	$0_1^+$	2290	100(2)	0.00198		0.22(4)	$B(E2) = 53(11)$
		$2_1^+$	1109	11.2(11)	0.0133	0.61(31)		$B(M1) = 0.014(7)$ $B(E2) = 60(29)$
2387	$3_1^-$	$0_1^+$	2387	1.0(3)	0.00309		0.50(6)	$B(E3) = 70(31) \times 10^3$
		$2_1^+$	1205	100.0(15)	0.00197			$B(E1) = 0.64(9) \times 10^{-3}$
		$4_1^+$	960	11.3(6)	0.00292			$B(E1) = 0.14(3) \times 10^{-3}$

<sup>a</sup> From ref. [18].

<sup>b</sup> Total electron conversion coefficients. From ref. [28].

<sup>c</sup> From ref. [28].

<sup>d</sup>  $B(E1)$  values are given in  $e^2\text{fm}^2$ ,  $B(E2)$  values are given in  $e^2\text{fm}^4$  (1 W.u. =  $74.15 e^2\text{fm}^4$ ),  $B(E3)$  value is given in  $e^2\text{fm}^6$ , and  $B(M1)$  value is given in  $\mu_N^2$ .

However, due to the isomeric nature of the  $4_1^+$ , the  $6_1^+$  and the  $8_1^+$  states the overall effect of their decays is that the 245 keV ( $4_1^+ \rightarrow 2_1^+$ ) transition is always emitted at rest in the present experiment. Indeed, as can be seen from the insets in fig. 5 the 245 keV  $\gamma$ -ray line show no indication of Doppler-shifted components in its shape. Hence, when the  $2_1^+$  state is fed from the  $4_1^+ \rightarrow 2_1^+$  transition it also always decays at rest which gives extra counts into the fully stopped component of the 1181 keV transition. In order to extract correctly the lifetime of the first  $2^+$  state of  $^{210}\text{Po}$  by means of the Doppler-shift attenuation method, the contribution of the  $\gamma$ -rays coming from the 245 keV transition to the fully stopped component of the 1181 keV transition has to be eliminated. The efficiency corrected number of counts in the 245 keV line are subtracted from the efficiency corrected number of counts in the stopped component of the 1181 keV transition. That procedure could be automatically carried out with APCAD by simultaneously fitting the 1181 and the 245 keV lines.

In addition, the  $\gamma$ - $\gamma$  coincidence data indicate the presence of 1427 keV transition which connects the  $0_2^+$  state at 2608 keV to the  $2_1^+$  state. However, this is an extremely weak transition which accounts for less than 1% of the total population of the  $2_1^+$  state and practically, has no impact on the lifetime of the  $2_1^+$  state. Therefore, besides the influence of the feeding from the  $4_1^+$ , the  $2_2^+$  and the  $3_1^-$  states, only fast feeding ( $\tau_{\text{feeding}} \leq 10$  fs) was considered in the fit of the line shape of 1181 keV transition. Under this assumption, the final value of the lifetime of the  $2_1^+$  is extracted from a simultaneous line-shape fit of the 1181 keV transition observed at forward and backward angles (see fig. 5) and presented in table 1.

## 4 Discussion

The lifetimes from the present study, together with the available spectroscopic information and the resulting transition strengths, are summarized in table 1. The lifetime for the  $3_1^-$  state of  $^{210}\text{Po}$  is in a good agreement with the estimated value from ref. [12]. The lifetime of the  $2_2^+$  state is measured for the first time. The new value for the  $2_1^+$  state is about a factor of three shorter than the adopted one [28]. The latter is deduced from a relative cross-section measurement in a ( $d, d'$ ) scattering experiment [12]. It has to be noted, however, that the new value is in a better agreement with the lifetime resulting from the cross-section for ( $p, p'$ ) scattering reported in the same study [12]. On the other hand, the value from the present study is obtained by a model-independent technique and free of the systematic uncertainties inherent to cross-section analysis.

The shorter lifetime of the  $2_1^+$  state leads to  $B(E2; 2_1^+ \rightarrow 0_1^+) = 1.83(28)$  W.u. which is about three times larger than the adopted value [12, 28]. However, this is not sufficient to compensate for the discrepancy between the experimental value and the estimations within the pure seniority scheme [29] or the shell model result (cf.

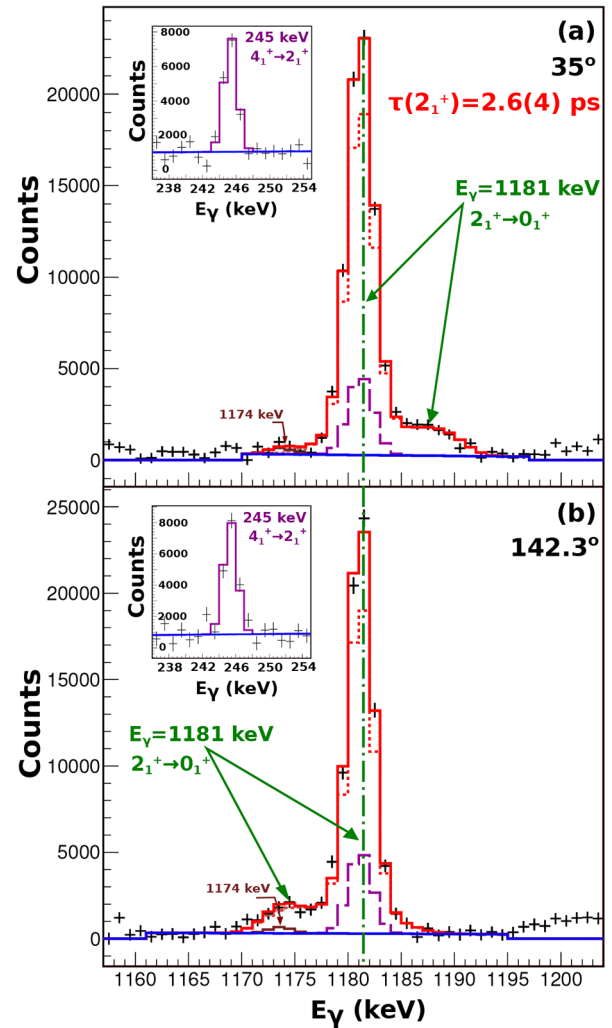


**Fig. 5.** (Color online) Simultaneous line-shape fits of the 1181 keV ( $2_1^+ \rightarrow 0_1^+$ ) transition observed at forward (a) and at backward (b) angles. The solid (red) line represents the total fit. The 1181 keV line is fitted simultaneously with the 245 keV ( $4_1^+ \rightarrow 2_1^+$ ) line which is always emitted from a stopped nucleus (the insets). The dotted and dashed lines represent the individual contributions of 1181 keV (red) and 245 keV (purple) lines, respectively, to the total fit. An unidentified stopped contaminant with  $E_\gamma = 1174$  keV is taken into account (brown).

table VII in ref. [13] and table III in ref. [14]) which remain two times larger than the experimental value. Since, at this point the discrepancy cannot be explained any longer as due to experimental uncertainties, the alternative that it results from the deficiencies of shell model [14] seems more likely. In ref. [14] the flaw is attributed to the neglect of  $ph$  excitations of the  $^{208}\text{Pb}$  core which strongly influence the  $J^\pi = 2^+$  states [30].

It is also interesting to check whether the problem is specific for shell models and whether other theoretical approaches can do better in describing the properties of low-lying states of  $^{210}\text{Po}$ . For this purpose we have performed Quasi-particle Phonon Model (QPM) calculations [16] for

**Table 2.** Results from the QPM calculations for the low-lying states of  $^{210}\text{Po}$  in comparison with the experimental data.

$J_i^\pi$	$E_x$ , (MeV)		Structure <sup>a</sup>	Transition strength <sup>b</sup>		
	Experiment	QPM		%	$J_f^\pi$	Experiment
$2_1^+$	1.18	1.10	97% $[2_1^+]_{RPA}$	$0_1^+$	$B(E2) = 136(21)$	$B(E2) = 135$ <sup>c</sup>
$4_1^+$	1.43	1.16	99% $[4_1^+]_{RPA}$	$2_1^+$	$B(E2) = 331(13)$ <sup>d</sup>	$B(E2) = 41$
$6_1^+$	1.47	1.20	99% $[6_1^+]_{RPA}$	$4_1^+$	$B(E2) = 227(5)$ <sup>e</sup>	$B(E2) = 28$
$8_1^+$	1.56	1.21	99% $[8_1^+]_{RPA}$	$6_1^+$	$B(E2) = 83(3)$ <sup>f</sup>	$B(E2) = 11$
$2_2^+$	2.29	2.05	1.2% $[2_1^+]_{RPA} + 60.5\%[2_1^+ \otimes 2_1^+]_{RPA} + 20.7\%[2_1^+ \otimes 4_1^+]_{RPA}$	$0_1^+$	$B(E2) = 53(11)$	$B(E2) = 3.4$
				$2_1^+$	$B(M1) = 0.014(7)$	$B(M1) = 0.006$
				$2_1^+$	$B(E2) = 60(29)$	$B(E2) = 80$
$3^-$	2.39	2.61	95% $[3_1^-]_{RPA}$	$0_1^+$	$B(E3) = 70(31) \times 10^3$	$B(E3) = 70 \times 10^3$
				$2_1^+$	$B(E1) = 0.64(9) \times 10^{-3}$	$B(E1) = 0.83 \times 10^{-3}$
				$4_1^+$	$B(E1) = 0.14(3) \times 10^{-3}$	$B(E1) = 0.27 \times 10^{-3}$

<sup>a</sup>  $[2_1^+]_{RPA}$  means the lowest in energy RPA phonon of the multipolarity  $2^+$ , etc.

<sup>b</sup>  $B(E1)$  values are given in  $e^2\text{fm}^2$ ,  $B(E2)$  values are given in  $e^2\text{fm}^4$  (1 W.u. =  $74.15 e^2\text{fm}^4$ ),  $B(E3)$  value is given in  $e^2\text{fm}^6$ , and  $B(M1)$  value is given in  $\mu_N^2$ .

<sup>c</sup> The strength of the quadrupole isoscalar residual interaction has been adjusted to the experimental  $B(E2, 2_1^+ \rightarrow 0_{g.s.})$  value in  $^{210}\text{Po}$ .

<sup>d</sup> From ref. [28].

<sup>e</sup> From ref. [11].

<sup>f</sup> From ref. [28].

$^{210}\text{Po}$ . In these calculations we have used the Woods-Saxon potential for the mean field with the parameters presented in ref. [31]. The single-particle space includes all shells from the potential bottom to quasibound states with narrow widths. The single-particle energies of the levels near the Fermi surface are taken from ref. [32], where they have been adjusted to reproduce experimental energies of low-lying levels of four odd-mass neighbouring nuclei to  $^{208}\text{Pb}$  in a calculation with the interactions between quasiparticles and phonons accounted for. The strength of the monopole pairing interaction for protons in  $^{210}\text{Po}$  has been adjusted to the corresponding even/odd mass differences. Because of the large single-particle model space no effective charges were used for calculating the  $E1$ ,  $E2$ , and  $E3$  transition strengths. The spin-gyromagnetic quenching factor used to calculate the  $M1$  transition strengths is  $g_s^{\text{eff}} = 0.8g_s^{\text{free}}$ . Excitation modes of even-even nuclei (both collective and almost two-quasi-particle ones) are treated in the QPM in terms of phonons. Their excitation energies and internal fermion structure is obtained from solving Quasi-particle Random-Phase Approximation (QRPA) equations. The model uses a separable form of the residual interaction. In the present studies we have used the Bohr-Mottelson form factor of the residual force as a derivative of the mean-field potential. The strength of the isoscalar residual interaction, the same for all multipoles, has been adjusted to the experimental  $B(E2, 2_1^+ \rightarrow 0_{g.s.})$  value in  $^{210}\text{Po}$ . The calculations have been performed on the basis of interacting one-, two-, and three-phonon configurations. The phonons of the  $2^+$ ,  $3^-$ ,  $4^+$ ,  $6^+$ , and  $8^+$  multipoles have been involved. Complex (two- and three-phonon) configurations have been built up from all possible combinations of these phonons. The basis has been truncated above 6 MeV, 8 MeV, and

10 MeV for one-, two-, and three-phonon components, respectively.

The results from the calculations are presented and compared to the experimental data in table 2. The energies of the states of interest are reasonably well reproduced but the lowest  $4^+$ ,  $6^+$ , and  $8^+$  states are practically degenerate in energy because of their almost pure  $\pi\{(1h_{9/2})^2\}$  nature. It has to be noted that in the chosen approach to fix the strength parameters to the electric strengths of the  $2_1^+$  state, the result for the energies of the states should be considered as a prediction of the model. In this respect, the agreement between the experimental and the calculated energies for the  $2_1^+$  and the  $3_1^-$  states allows to interpret them as one-quadrupole and one-octupole phonon states, respectively. The energies of the  $4_1^+$ ,  $6_1^+$ , and  $8_1^+$  states are somewhat lower in the calculation than experimentally observed. It should be noted that the energy of the lowest two-quasiparticle configuration  $\pi\{(1h_{9/2})^2\}$  is 1.211 MeV with the present quasiparticle spectrum. In general, the calculation predicts a rather pure one-phonon nature of the lowest  $2^+$ ,  $4^+$ ,  $6^+$  and  $8^+$  states.

The major discrepancy between the QPM calculations and the experimental data appears in the  $E2$  transition strengths for the cascade  $8_1^+ \rightarrow 6_1^+ \rightarrow 4_1^+$  (cf. table 2). Overall, the model underestimates these values by a factor of 8. Since the corresponding states have a rather pure one-phonon nature, these transitions are determined by the  $E2$  matrix elements  $\langle [6_1^+]_{RPA} || E2 || [8_1^+]_{RPA} \rangle$ , etc. These matrix elements are much smaller as compared to the decays from two-phonon components  $\langle [6_1^+]_{RPA} || E2 || [2_1^+ \otimes 6_1^+]_{RPA} \rangle$ , etc. with an exchange of the  $[2_1^+]_{RPA}$  phonon [33]. Experimental data definitely indicate strong admixture of two phonon components in the structure of the  $4_1^+$ ,  $6_1^+$ , and  $8_1^+$  states which

is not reproduced in the QPM calculations. The problem existing in the shell model description also appears in a different form in the present QPM calculations. This may indicate that the  $^{208}\text{Pb}$  core is soft as this softness strongly enhances the  $1ph$  excitations, or facilitates the mixing between the  $2qp$  configurations. Obviously, neither shell models nor QPM account correctly for this peculiarity.

## 5 Conclusions

In the present study the lifetimes of the  $2_1^+$ , the  $2_2^+$  and the  $3_1^-$  states of  $^{210}\text{Po}$  have been measured by the Doppler-shift attenuation method. The newly established value of the lifetime of the  $2_1^+$  state leads to an  $E2$  transition strength which is about three times larger than the adopted value [28]. However, the newly measured value is still not high enough to allow for a consistent microscopic description of the properties of the yrast  $2_1^+$ ,  $4_1^+$ ,  $6_1^+$ , and  $8_1^+$  states of  $^{210}\text{Po}$  using  $^{208}\text{Pb}$  as an inert core. Such description is well expected since  $^{210}\text{Po}$  comprises only two additional protons with respect to the doubly magic nucleus  $^{208}\text{Pb}$ . The problem previously known from shell model studies also appears in the performed QPM calculations. This observation and the new experimental value for the lifetime of the  $2_1^+$  state prompt for a more thorough theoretical investigation of this problem.

DK acknowledges the support from Deutscher Akademischer Austauschdienst. This work was supported by the partnership agreement between the University of Cologne and University of Sofia, by the BgNSF under grant DN08/23/2016, by STFC, by the German-Bulgarian exchange program under grants PPP57082997 & DNTS/01/05/2014, by the DFG under grant SFB 1245, and by the BMBF under grants 05P12RDCIB, 05P15RDFN1,9 and 05P15RDCIA.

## References

1. M. Goeppert-Mayer, Phys. Rev. **78**, 16 (1950).
2. M.G. Mayer, J.H.D. Jensen, *Elementary Theory of Nuclear Shell Structure* (John Wiley & Sons, Inc., 1955).
3. G. Racah, Phys. Rev. **63**, 367 (1943).
4. A. de Shalit, I. Talmi, *Nuclear Shell Theory* (Academic Press, New York, 1963) p. 283.
5. I. Talmi, *Simple Models of Complex Nuclei. The Shell Model and Interacting Boson Model* (Harwood, Chur, 1993).
6. Igal Talmi, Nucl. Phys. A **172**, 1 (1971).
7. R.F. Casten, *Nuclear Structure from a Simple Perspective* (Oxford University Press, New York, 2000).
8. J.J. Ressler *et al.*, Phys. Rev. C **69**, 034317 (2004).
9. J.J. Ressler *et al.*, Phys. Rev. C **69**, 034331 (2004).
10. T. Grahn *et al.*, Eur. Phys. J. A **52**, 340 (2016).
11. O. Häusser *et al.*, Nucl. Phys. A **273**, 253 (1976).
12. C. Ellegaard *et al.*, Nucl. Phys. A **206**, 83 (1973).
13. L. Coraggio *et al.*, Phys. Rev. C **60**, 064306 (1999).
14. E. Caurier, M. Rejmund, H. Grawe, Phys. Rev. C **67**, 054310 (2003).
15. T.K. Alexander, J.S. Forster, Adv. Nucl. Phys. **10**, 197 (1978).
16. V.G. Soloviev, *Theory of Atomic Nuclei, Quasiparticles and Phonons* (IOP, London, 1992).
17. A. Dewald, O. Möller, P. Petkov, Prog. Part. Nucl. Phys. **67**, 786 (2012).
18. L.G. Mann *et al.*, Phys. Rev. C **38**, 74 (1988).
19. C. Stahl, J. Leske, M. Lettmann, N. Pietralla, Comput. Phys. Commun. **214**, 174 (2017).
20. S. Agostinelli *et al.*, Nucl. Instrum. Methods Phys. Res. A **506**, 250 (2003).
21. L.C. Northcliffe, R.F. Schilling, Nucl. Data Tables **7**, 233 (1970).
22. J.F. Ziegler, J.P. Biersack, in *Treatise on Heavy Ion Science*, Vol. **6**, edited by D.A. Bromley (Plenum Press, New York, 1985) p. 95.
23. J.F. Ziegler, M.D. Ziegler, J.P. Biersack, Nucl. Instrum. Methods B **268**, 1823 (2010).
24. J. Keinonen, AIP Conf. Proc. **125**, 557 (1985).
25. D. Kocheva *et al.*, Phys. Rev. C **93**, 011303(R) (2016).
26. A. Astier, P. Petkov, M.-G. Porquet, D.S. Delion, P. Schuck, Phys. Rev. Lett. **104**, 042701 (2010).
27. A. Astier, P. Petkov, M.-G. Porquet, D.S. Delion, P. Schuck, Eur. Phys. J. A **46**, 165 (2010).
28. M. Shamsuzzoha Basunia, Nucl. Data Sheets **121**, 561 (2014).
29. A.E. Stuchbery, AIP Conf. Proc. **1625**, 52 (2014).
30. F. Nowacki, Nucl. Phys. A **704**, 223 (2002).
31. C.A. Bertulani, V.Yu. Ponomarev, Phys. Rep. **321**, 139 (1999).
32. V.V. Voronov, Dao Tien Khoa, Izv. Akad. Nauk SSSR, Ser. Fiz. **48**, 2008 (1984).
33. V.Yu. Ponomarev, Ch. Stoyanov, N. Tsoneva, M. Grinberg, Nucl. Phys. A **635**, 470 (1998).